Desalination and Water Treatment
www.deswater.com

doi: 10.5004/dwt.2023.29737

300 (2023) 230–236
July

Photocatalytic performance of Ag_3PO_4/BiOBr heterojunctions induced by effective interfacial charge separation

Qian Zhang†, Youmei Li†, Junbo Zhong*, Jianzhang Li*

Key Laboratory of Green Catalysis of Higher Education Institutes of Sichuan, School of Chemistry and Environmental Engineering, Sichuan University of Science and Engineering, Zigong 643000, P.R. China, emails: junbozhong@163.com/lschmanuscipt@163.com (J. Zhong), lyl63@sina.com (J. Li), 1144049472@qq.com (Q. Zhang), 2509132838@qq.com (Y. Li)

Received 6 December 2021; Accepted 29 July 2023

ABSTRACT

In this work, Ag_3PO_4/BiOBr heterojunction photocatalyst was prepared by a precipitation method. The formation of Ag_3PO_4/BiOBr heterojunctions was proven by X-ray diffraction, energy-dispersive X-ray spectroscopy and high-resolution transmission electron microscopy. The as-prepared samples were characterized by scanning electron microscopy, UV-Vis diffuse reflectance spectrum and Brunauer–Emmett–Teller surface area. Separation behaviors of photoinduced carriers were investigated by surface photovoltage spectroscopy, the results display that the separation rate of photoinduced carriers of Ag_3PO_4/BiOBr heterojunctions was significantly promoted. The activities of the photocatalysts were evaluated by destruction of Rhodamine B (RhB) and methyl orange (MO). The results exhibit that the photocatalytic performance of Ag_3PO_4/BiOBr photocatalyst is higher than that of the reference BiOBr. The degradation rate constant of RhB and MO over Ag_3PO_4/BiOBr is about 3 and 2.8 times of that on the reference BiOBr under visible light irradiation, respectively, which can be attributed to the significantly promoted light response capacity to visible light and enhanced separation efficiency of photo-generated carriers of BiOBr originated from the coupling of Ag_3PO_4 and BiOBr. In view of the observations, photocatalytic enhancement mechanism of Ag_3PO_4/BiOBr was proposed.

Keywords: Heterojunctions; Ag_3PO_4/BiOBr; Semiconductors; Charge separation

1. Introduction

Nowadays, with the rapid development of industrial technology and the social economy, a large number of toxic organic pollutants are directly discharged into the atmosphere, water, and soil, which becomes a serious threat to human life and social-economic development [1,2]. For instance, Rhodamine B (RhB) and methyl orange (MO) are two typical organic dyes, which may form serious menaces to human health and ecosystem since they have been widely used in various industries and their carcinogenic and deformity [3]. Recently, photocatalysis has attracted widespread attention due to its ability to directly utilize solar energy for energy conversion and environmental purification [4,5]. Therefore, it is of great significance to seek highly active photocatalysts with broad-spectrum absorption efficiency, rapid carrier transfer efficiency, long-term stability, and lifetime [6,7].

As a novel visible-light driven photocatalyst, BiOBr has received increasing attention due to its excellent chemical stability, suitable band gap and special hierarchical structure [8–14]. However, because of its low light quantum efficiency, the photocatalytic activity of BiOBr is still low, which greatly restricts its practical applications. According to previous reports [15–21], the heterojunctions constructed by BiOBr and other semiconductor materials

* Corresponding author.
† These authors contributed equally to this work.

exhibit excellent photocatalytic activity, such as Fe_3O_4/BiOBr [22], BiOBr/$BiOIO_3$ [23], $BiVO_4$/BiOBr [24] and so on. Among the existed photocatalysts, Ag_3PO_4 is an ideal candidate to couple with BiOBr [25,26]. Bandgap of Ag_3PO_4 is 2.4 eV, and the corresponding absorption threshold is about 525 nm [27,28], which can well absorb visible light. In addition, Ag_3PO_4 has relatively high oxidation ability and can effectively degrade organic pollutant molecules under visible light irradiation. It has been reported that a graphene wrap BiOBr/Ag_3PO_4 Z-scheme heterojunction was successively synthesized by solvothermal and precipitation method. The as-obtained BiOBr/Ag_3PO_4@rGO composite presents excellent photocatalytic activity and mineralization ability for TC degradation. The stack disorder which cased by the intercalation of BiOBr and Ag_3PO_4 into two-dimensional stacked rGO thin layers is beneficial for increasing photocatalytic activity. But in fact, BiOBr/Ag_3PO_4 also performed higher photocatalytic performance than BiOBr in this report, which is nearly 2.2-folds of that of the reference BiOBr [29]. Besides, separation behaviors of photoinduced carriers haven't been investigated by surface photovoltage spectroscopy (SPS).

Herein, in this work, Ag_3PO_4/BiOBr composite photocatalyst was *in-situ* prepared by a precipitation approach [30–34]. Using RhB and MO as model pollutants, photocatalytic activity and stability of the catalyst were investigated. The interfacial charge separation behavior of the Ag_3PO_4/BiOBr composite was thoroughly investigated. The promoted photocatalytic performance of Ag_3PO_4/BiOBr can be allocated to the effective separation of photoinduced carriers.

2. Experimental section

2.1. Preparation of BiOBr

BiOBr nanosheets were synthesized via a hydrothermal method. 0.01 mol $Bi(NO_3)_3{\cdot}5H_2O$ was added into 40 mL glacial acetic acid, and solution A was obtained by ultrasonification for 10 min. 0.01 mol KBr was added into 20 mL deionized water and stirred for 5 min to obtain solution B. Solution B was slowly added to solution A dropwise and continued to stir for 30 min. The resulting milky suspension was then transferred to a 100 mL polytetrafluoroethylene reactor for microwave hydrothermal reaction at 180°C for 2 h. After cooling to room temperature, the obtained product was washed with deionized water and anhydrous ethanol for three times, respectively, and then was dried in an oven at 60°C for 24 h to obtain BiOBr.

2.2. Preparation of Ag_3PO_4/BiOBr heterojunctions

Ag_3PO_4/BiOBr heterojunctions were synthesized *in-situ* via a precipitation method. 1.0065 g BiOBr was dispersed into 40 mL deionized water, and the suspension solution was obtained by sonicating for 30 min. Then, 0.1700 g $AgNO_3$ was added into the suspension in dark. After stirring for 30 min, 10 mL Na_3PO_4 solution containing 0.1267 g $Na_3PO_4{\cdot}12H_2O$ was added dropwise to the above suspension and was continuously stirred at room temperature for 4 h. After filtration, the product was rinsed with deionized water and absolute ethanol for three times, respectively, and then was dried in an oven at 60°C for 24 h to obtain Ag_3PO_4/BiOBr heterojunctions. To ensure consistent experimental conditions, Ag_3PO_4 was obtained according to the above steps without adding of BiOBr.

2.3. Evaluation of photocatalytic activity

In this work, the performance of photocatalysts was measured by destruction of simulated organic pollutants in sewage using a Xe lamp (PLS-SXE 300C 300 W) with a cut-off filter (λ > 420 nm) to remove ultraviolet light. The simulated sewage was RhB and MO aqueous solution (10 mg/L). 0.05 g the prepared catalyst was put into 50 mL RhB or MO aqueous solution, respectively. The mixture containing quantitative sample and RhB or MO was stirred for 30 min in dark to acquire an adsorption–desorption equilibrium. To monitor the concentration of pollutants, after a specific irradiation interval, 5 mL suspension was taken out and the powder was moved from the suspension solution by high-speed centrifugation. A 756 P C spectrophotometer was used to determine the absorbance of RhB and MO solution at 554 and 464 nm, respectively.

3. Results and discussion

3.1. Characterization of the samples

To investigate the effect of construction of heterojunction on the specific surface area Brunauer–Emmett–Teller of the catalyst, the S_{BET} of samples was detected and is presented in Table 1. The specific surface area of Ag_3PO_4/BiOBr heterojunctions is higher than that of BiOBr. The enhancement in specific surface area is probably due to the existence of Ag_3PO_4 on the surface of BiOBr. Commonly, high specific surface area is favorable for the photocatalytic activity.

Fig. 1 shows the X-ray diffraction (XRD) patterns of BiOBr, Ag_3PO_4 and Ag_3PO_4/BiOBr heterojunctions. It can be seen that all the diffraction peaks of the pure BiOBr and Ag_3PO_4 correspond to the standard BiOBr XRD card (JCPDS No.09-0393) and the standard Ag_3PO_4 XRD card (JCPDS No.06-0505). In addition, for Ag_3PO_4/BiOBr heterojunctions, the diffraction peaks of BiOBr and Ag_3PO_4 can be observed simultaneously, indicating that Ag_3PO_4 and BiOBr have successfully combined. In order to further investigate the microstructure of the prepared samples, scanning electron microscopy (SEM) and high-resolution transmission electron microscopy (HRTEM) measurements were carried out.

From Fig. 2a it can be found that BiOBr is nanosheets (about 1–2 μm) with a smooth surface. In Fig. 2b many irregular Ag_3PO_4 nanoparticles were successfully deposited on the surface of BiOBr. Energy-dispersive X-ray (EDS) spectrum of Ag_3PO_4/BiOBr is shown in Fig. 2c. It is apparent that the characteristic peaks for elements such as Ag, O, Bi and Br appear in the spectrum, further indicating that Ag_3PO_4 and BiOBr coexist in the heterojunctions. From

Table 1
Specific surface area of samples

Sample	BiOBr	Ag_3PO_4/BiOBr
S_{BET} (m^2/g)	3.8	4.0

the HRTEM of the Ag_3PO_4/BiOBr sample demonstrated in Fig. 2d, the lattice spacing of 0.2138 nm and 0.1984 nm corresponds to the (220) crystal plane of the cubic phase Ag_3PO_4 and the (200) crystal plane of the tetragonal phase BiOBr, respectively. The HRTEM result is in good agreement with the results obtained by XRD, SEM, and EDS. These results prove that Ag_3PO_4 was successfully loaded on the surface of BiOBr.

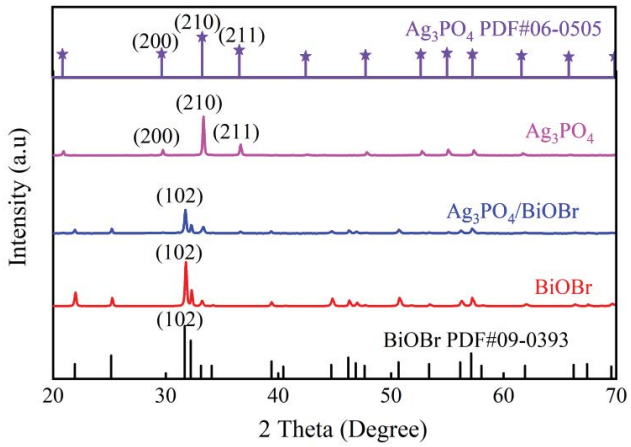

Fig. 1. X-ray diffraction patterns of the photocatalysts.

Fig. 3a is the UV-Vis diffuse reflectance spectrum (UV-Vis DRS) spectra of the sample. It can be seen that the absorption threshold of the pristine BiOBr is about 450 nm, which is consistent with previous reports [15]. Compared with BiOBr, the visible light absorption capacity of Ag_3PO_4/BiOBr heterojunction is significantly enhanced, indicating that the existence of Ag_3PO_4 expands the light response range of the catalytic material to visible light, which is beneficial to the improvement of photocatalytic performance. The bandgap of the semiconductor can be calculated by the following formula:

$$(\alpha h\nu)^{n/2} = A(h\nu - E_g) \quad (1)$$

where α is the absorption coefficient, h is Planck's constant, v is the light frequency, A is a constant [35] and n is an index that depends on the electronic transition of the semiconductor [36] (n = 1 for direct-gap semiconductor, n = 4 for indirect-gap semiconductor [23]). For Ag_3PO_4 and BiOBr, the n value represents 1 and 4, respectively. As shown in Fig. 3b, the bandgap (E_g) for BiOBr and Ag_3PO_4 is estimated to be 2.63 and 2.16 eV by plotting $(\alpha hv)^{1/2}$ and $(\alpha hv)^2$ vs. hv, respectively, which is close to the previous report [29].

Fig. 4a shows the SPS spectra of BiOBr and Ag_3PO_4/BiOBr composite photocatalyst. It can be seen from Fig. 4a that the original BiOBr only responds to light in the range

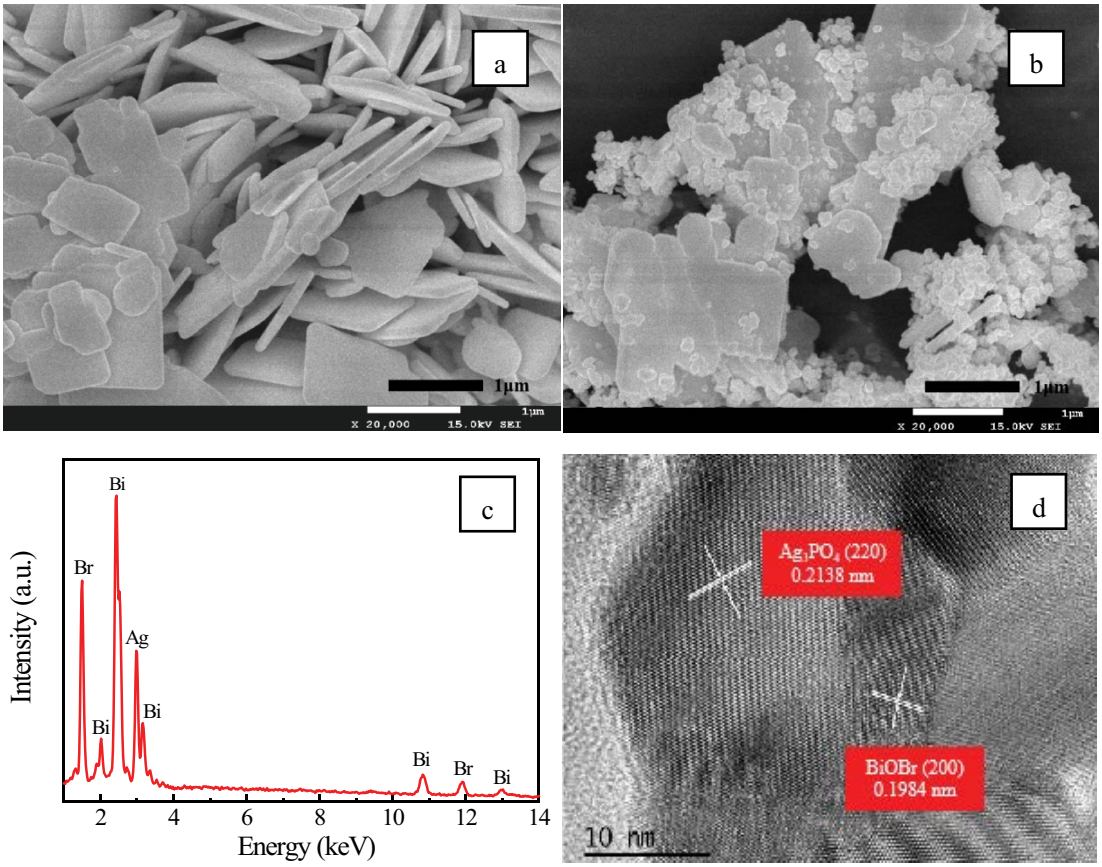

Fig. 2. Scanning electron microscopy images of (a) BiOBr, (b) Ag_3PO_4/BiOBr, (c) energy-dispersive X-ray spectrum of Ag_3PO_4/BiOBr, (d) high-resolution transmission electron microscopy of Ag_3PO_4/BiOBr.

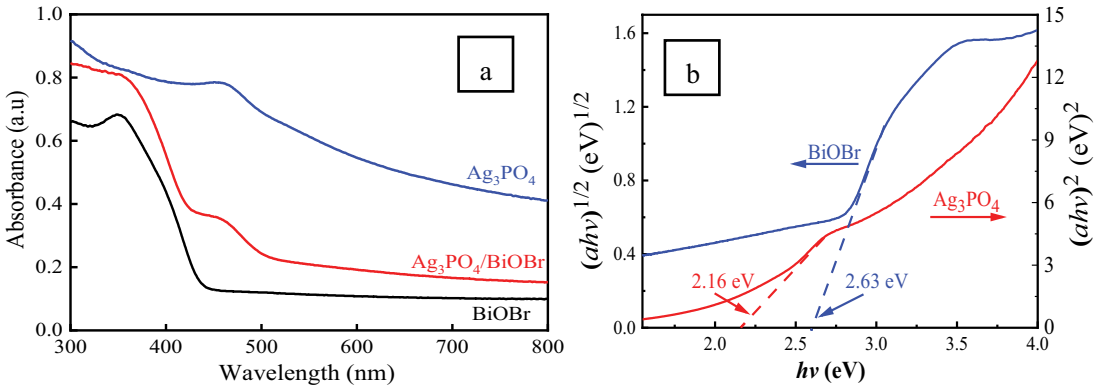

Fig. 3. (a) UV-Vis diffuse reflectance spectra and (b) corresponding bandgap of the different samples.

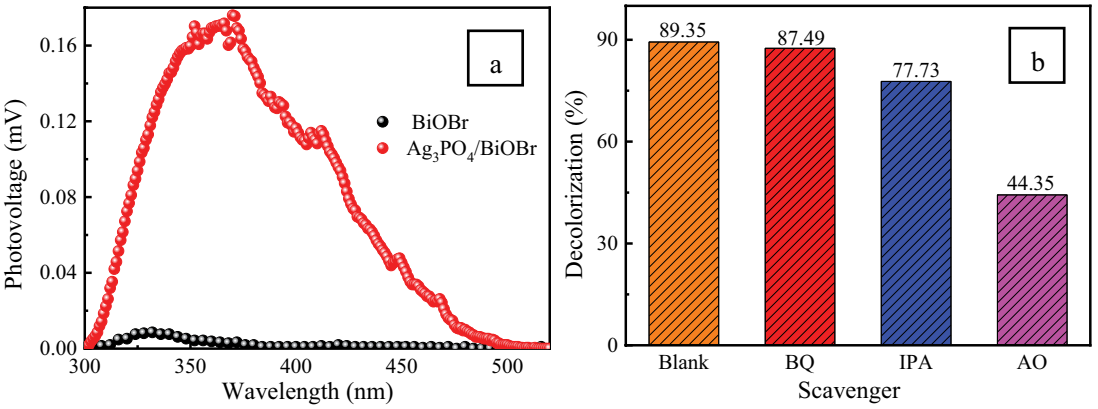

Fig. 4. (a) Surface photovoltage spectra of the photocatalysts and (b) effects of the different scavengers on photocatalytic degradation of Rhodamine B and methyl orange over Ag_3PO_4/BiOBr under visible light irradiation.

of 300–400 nm. After coupling with Ag_3PO_4, light response range of the heterojunctions has significantly expanded to about 500 nm, indicating that the Ag_3PO_4/BiOBr composite has a stronger visible-light absorption capacity than the single BiOBr, which is consistent with the results obtained by UV-Vis DRS. According to the detection principle of SPS experiment, the intensity of SPS signal corresponds to the separation rate of photocarriers [37]. In addition, the prepared Ag_3PO_4/BiOBr composite photocatalyst exhibits a stronger SPS signal than BiOBr. BiOBr shows SPS response from 300–400 nm, however, Ag_3PO_4/BiOBr composite displays strong SPS signal from 300–500 nm, it is evident that the strong and boosted SPS signals of Ag_3PO_4/BiOBr stems from the presence of Ag_3PO_4 in the composite. Coupling Ag_3PO_4 with BiOBr can establish an interfacial electric field due to the different Fermi levels and work functions of two photocatalysts, facilitating the separation of photoinduced carriers. Generally, high separation efficiency of photoinduced carriers is favorable for the photocatalytic performance.

To ascertain the role of the active free radicals, trapping experiments were executed. Benzoquinone (BQ) was selected as the $^{\bullet}O_2^-$ trapping agent, isopropanol (IPA) as the $^{\bullet}OH$ trapping agent, and ammonium oxalate (AO) as h^+ trapping agent. The experimental results were shown in Fig. 4b. It can be observed that addition of benzoquinone has no significant effect on the catalytic activity of the Ag_3PO_4/BiOBr photocatalyst. Addition of ammonium oxalate and isopropanol significantly inhibits the degradation of RhB over the catalyst, indicating that h^+ and $^{\bullet}OH$ are the main active species in the photocatalytic reaction process.

3.2. Photocatalytic performance

Photocatalytic activity of the photocatalysts is shown in Fig. 5a and b. After coupling BiOBr with Ag_3PO_4, photocatalytic performance of Ag_3PO_4/BiOBr heterojunction photocatalyst has been significantly improved under visible light irradiation. The results in Fig. 5c and d further show that the degradation rate constant of RhB and MO over Ag_3PO_4/BiOBr is about 3 and 3.5 times of that on the pristine BiOBr, respectively. From the obtained results, it is apparent that construction of heterojunctions can expand the utilization range of BiOBr for visible light and significantly increase the efficiency of photo-generated electron–hole separation, thereby significantly enhancing its photocatalytic performance.

Fig. 6 presents the stability test results of the Ag_3PO_4/BiOBr catalyst. After 4 repeated experiments, the degradation efficiency of RhB over the catalyst samples is 90.17%, 85.25%, 78.38% and 72.89%, respectively. After four cyclic

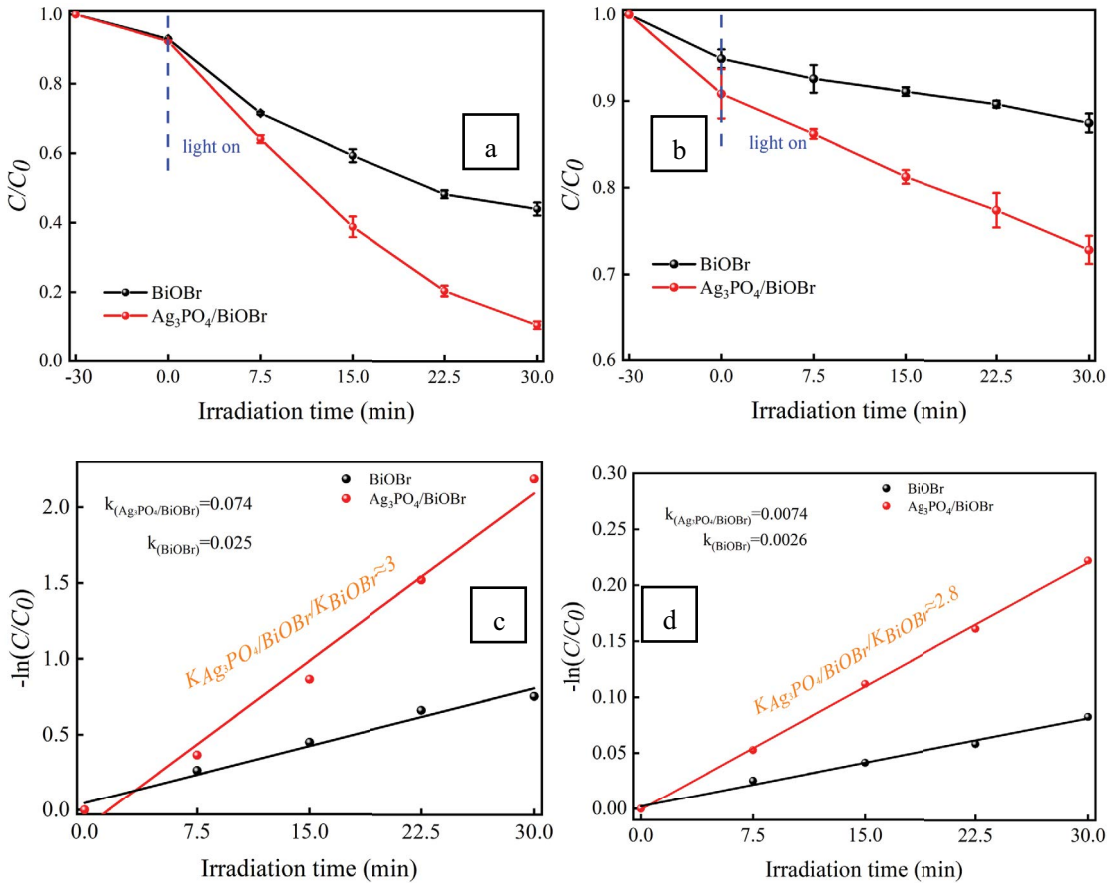

Fig. 5. Photocatalytic activities of BiOBr and Ag_3PO_4/BiOBr heterostructures toward degradation of (a) Rhodamine B and (b) methyl orange under visible light irradiation; Fitted first-order kinetic for Rhodamine B (c) and methyl orange (d).

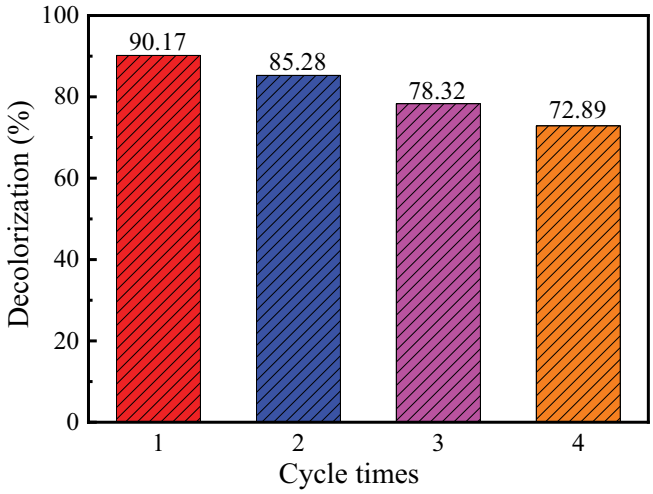

Fig. 6. Stability of the Ag_3PO_4/BiOBr photocatalyst under the visible-light irradiation.

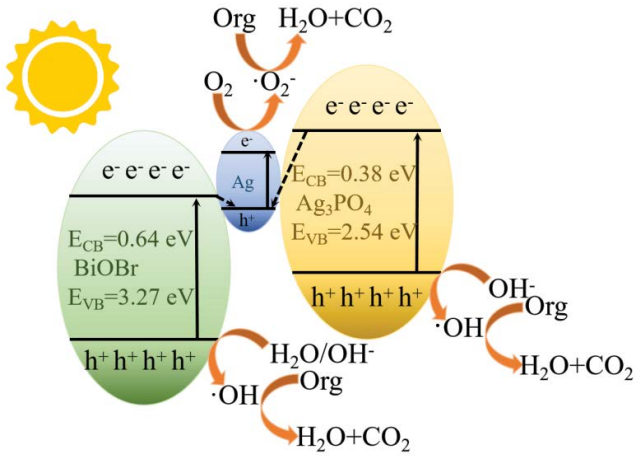

Fig. 7. Photocatalytic mechanism of Ag_3PO_4/BiOBr heterojunctions.

experiments, the catalytic efficiency decreases by about 20%. This may be due to the fall of Ag_3PO_4 from the BiOBr surface during the experiment, which reduces the photocatalytic performance of the sample.

3.3. Photocatalytic mechanism

To explore the photocatalytic mechanism, the relative position of the valance band (VB) and conduction band (CB) of BiOBr and Ag_3PO_4 were estimated by Mulliken electronegativity formula as follows:

$$E_{VB} = X - E_e + 0.5E_g \quad (2)$$

$$E_{CB} = E_{VB} - E_g \quad (3)$$

where E_{VB} and E_{CB} is the potential valance band and conduction band, respectively. X is the absolute electronegativity of the semiconductor, E_e is the energy of free electrons on the hydrogen scale (about 4.5 eV). The value of *X* for BiOBr and Ag_3PO_4 is 6.45 and 5.96 eV [28,38], respectively. Therefore, the E_{VB} and E_{CB} for BiOBr is evaluated to be 3.27 and 0.64 eV, respectively, the E_{VB} and E_{CB} of Ag_3PO_4 is calculated to be 2.54 and 0.38 eV, respectively.

In light of the above characterizations and photocatalytic performance assessment results, it is distinct that construction of BiOBr/Ag_3PO_4 heterostructures can promote the separation of photo-induced charge pairs. The photocatalytic mechanism for Ag_3PO_4/BiOBr heterojunctions is presented in Fig. 7. Ag^0 from Ag_3PO_4 under light irradiation can promote the separation of e^-/h^+ pairs and improve photocatalytic activity of the materials due to the surface plasmon resonance effect (SPR). Metal SPR can expedite the separation of photoexcited carriers, which can propagate along the metal surface [39]. Therefore, it is anticipated that ternary Ag/Ag_3PO_4/BiOBr heterojunctions will display higher photocatalytic activity than the reference BiOBr. The electrons from Ag^0 nanoparticles can react with O_2 to generate $^{\bullet}O_2^-$ ($E(^{\bullet}O_2^-/O_2)$ is 0.33 eV vs. NHE) [40]. The photogenerated holes from BiOBr can oxidize H_2O/OH^- to form $^{\bullet}OH$ radicals. However, the photogenerated holes of Ag_3PO_4 only can oxidize OH^- to form $^{\bullet}OH$ radicals ($E(^{\bullet}OH/OH^-)$ is 1.99 eV vs. NHE and $E(^{\bullet}OH/H_2O)$ is 2.68 eV vs. NHE) [41,42], $^{\bullet}OH$ can participate in the photocatalytic degradation of RhB and MO. Therefore, the as-prepared Ag_3PO_4/BiOBr heterojunctions follow double S-scheme mechanism, which can markedly boost the separation and transfer of photo-generated electrons and holes.

4. Conclusions

In summary, Ag_3PO_4/BiOBr heterojunctions were *in-situ* synthesized by a precipitation method. Combination of Ag_3PO_4 and BiOBr can significantly expand light response range. The interfacial electric field between two semiconductors can effectively improve the photo-generated electron–hole separation efficiency. Under visible light irradiation, Ag_3PO_4/BiOBr exhibits higher activity than BiOBr, which is nearly 3-fold of that of the reference BiOBr. The separation and transfer of photoinduced carriers follow S-scheme mechanism. This study offers a highly efficient photocatalyst for environmental purification.

Acknowledgments

This work was financially supported by Science and Technology Department of Sichuan Province (No. 2019YJ0457, No. 2021YFG0278, No. 2019ZYZF0069), Chemical Synthesis and Pollution Control Key Laboratory of Sichuan Province (CSPC201903, CSPC202105) and Key Laboratory of Catalysis and Energy Materials Chemistry of Ministry of Education & Hubei Key Laboratory of Catalysis and Materials Science (CHCL20005).

References

[1] W. Wang, Q. Niu, G. Zeng, C. Zhang, D. Huang, B. Shao, C. Zhou, Y. Yang, W. Xiong, L. Lei, S. Liu, H. Yi, S. Chen, X. Tang, 1D porous tubular g-C_3N_4 capture black phosphorus quantum dots as 1D/0D metal-free photocatalysts for oxytetracycline hydrochloride degradation and hexavalent chromium reduction, Appl. Catal., B, 273 (2020) 119051, doi: 10.1016/j.apcatb.2020.119051.

[2] L. Shan, J. Li, Z. Wu, L. Dong, H. Chen, D. Li, J. Suriyaprakash, X. Zhang, Unveiling the intrinsic band alignment and robust water oxidation features of hierarchical $BiVO_4$ phase junction, Chem. Eng. J., 436 (2022) 131516, doi: 10.1016/j.cej.2021.131516.

[3] M. Madadi, M. Ghorbanpour, A. Feizi, Preparation and characterization of solar light-induced rutile Cu-doped TiO_2 photocatalyst by solid-state molten salt method, Desal. Water Treat., 145 (2019) 257–261.

[4] M. Sridharan, T. Maiyalagan, Recent progress in tungsten disulphide based photocatalyst for hydrogen production and environmental remediation, Chem. Eng. J., 3 (2021) 130393, doi: 10.1016/j.cej.2021.130393.

[5] J. Yi, K. Wu, H. Wu, J. Guo, L. Zhang, H. Li, J. Li, Synthesis of novel g-C_3N_4/NH_2-MIL-88B(Fe) composite photocatalysis for efficient ciprofloxacin degradation under simulated sunlight irradiation, Nano, 6 (2021) 2150063, doi: 10.1142/S1793292021500636.

[6] J. Wang, Z. Chen, G. Zhai, Y. Men, Boosting photocatalytic activity of WO_3 nanorods with tailored surface oxygen vacancies for selective alcohol oxidations, Appl. Surf. Sci., 462 (2018) 760–771.

[7] Y. Feng, H. Li, L. Ling, S. Yan, D. Pan, H. Ge, H. Li, Z. Bian, Enhanced photocatalytic degradation performance by fluid-induced piezoelectric field, Environ. Sci. Technol., 52 (2018) 7842–7848.

[8] L. Shan, Y. Liu, H. Chen, Z. Wu, Z. Han, An α-Bi_2O_3/BiOBr core-shell heterojunction with high photocatalytic activity, Dalton Trans., 46 (2017) 2310–2321.

[9] X. Wang, G. Xu, Y. Tu, D. Wu, A. Li, X. Xie, BiOBr/PBCD-B-D dual-function catalyst with oxygen vacancies for Acid Orange 7 removal: evaluation of adsorption-photocatalysis performance and synergy mechanism, Chem. Eng. J., 411 (2021) 128456, doi: 10.1016/j.cej.2021.128456.

[10] X. Chen, X. Zhang, Y. Li, M. Qi, Y. Xu, Transition metal doping BiOBr nanosheets with oxygen vacancy and exposed {102} facets for visible light nitrogen fixation, Appl. Catal., B, 281 (2021) 119516, doi: 10.1016/j.apcatb.2020.119516.

[11] H. Yu, J. Huang, L. Jiang, Y. Shi, K. Yi, W. Zhang, J. Zhang, H. Chen, X. Yuan, Enhanced photocatalytic tetracycline degradation using N-CQDs/OV-BiOBr composites: unraveling the complementary effects between N-CQDs and oxygen vacancy, Chem. Eng. J., 402 (2020) 126187, doi: 10.1016/j.cej.2020.126187.

[12] X. Li, J. Xiong, X. Gao, J. Ma, Z. Chen, B. Kang, J. Liu, H. Li, Z. Feng, J. Huang, Novel BP/BiOBr S-scheme nanoheterojunction for enhanced visible-light photocatalytic tetracycline removal and oxygen evolution activity, J. Hazard. Mater., 387 (2020) 121690, doi: 10.1016/j.jhazmat.2019.121690.

[13] J. Guo, X. Liao, M. Lee, G. Hyett, C. Huang, D. Hewak, S. Mailis, W. Zhou, Z. Jiang, Experimental and DFT insights of the Zn-doping effects on the visible-light photocatalytic water splitting and dye decomposition over Zn-doped BiOBr photocatalysts, Appl. Catal., B, 243 (2019) 502–512.

[14] X. Lv, D. Yan, L. Lam, H. Yun, A. An, Solvothermal synthesis of copper-doped BiOBr microflowers with enhanced adsorption and visible-light driven photocatalytic degradation of norfloxacin, Chem. Eng. J., 401 (2020) 126012, doi: 10.1016/j.cej.2020.126012.

[15] W. Deng, F. Pan, B. Batchelor, B. Jung, P. Zhang, A. Abdelwahab, H. Zhou, Y. Li, Mesoporous TiO_2-BiOBr microspheres with tailorable adsorption capacities for photodegradation of organic water pollutants: probing adsorption-photocatalysis synergy by combining experiments and kinetic modeling, Environ. Sci. Water Res. Technol., 4 (2019) 769–781.

[16] Y. Shang, T. Wang, Y. Xiao, B. Li, Constructing BiOBr/CoO_X/g-C_3N_4 Z-scheme photocatalyst with CoO_X as both redox mediator and cocatalyst for phenol degradation, J. Alloys Compd., 875 (2021) 159998, doi: 10.1016/j.jallcom.2021.159998.
[17] Y. Chen, H. Tian, W. Zhu, X. Zhang, R. Li, C. Chen, Y. Huang, L-cysteine directing synthesis of BiOBr nanosheets for efficient cefazolin photodegradation: the pivotal role of thiol, J. Hazard. Mater., 414 (2021) 125544, doi: 10.1016/j.jhazmat.2021.125544.
[18] G. Li, S. Huang, N. Zhu, H. Yuan, D. Ge, Near-infrared responsive upconversion glass-ceramic@BiOBr heterojunction for enhanced photodegradation performances of norfloxacin, J. Hazard. Mater., 403 (2021) 123981, doi: 10.1016/j.jhazmat.2020.123981.
[19] J. Lyu, Z. Hu, Z. Li, M. Ge, Removal of tetracycline by BiOBr microspheres with oxygen vacancies: combination of adsorption and photocatalysis, J. Phys. Chem. Solids, 129 (2019) 61–70.
[20] L. Zhang, X. Yue, J. Liu, J. Feng, Facile synthesis of Bi_5O_7Br/BiOBr 2D/3D heterojunction as efficient visible-light-driven photocatalyst for pharmaceutical organic degradation, Sep. Purif. Technol., 231 (2019) 115917, doi: 10.1016/j.seppur.2019.115917.
[21] J. Wu, Y. Xie, Y. Ling, J. Si, X. Li, J. Wang, H. Ye, J. Zhao, S. Li, Q. Zhao, Y. Hou, One-step synthesis and Gd^{3+} decoration of BiOBr microspheres consisting of nanosheets toward improving photocatalytic reduction of CO_2 into hydrocarbon fuel, Chem. Eng. J., 400 (2020) 125944, doi: 10.1016/j.cej.2020.125944.
[22] S. Li, Z. Wang, X. Zhang, J. Zhao, Z. Hu, Z. Wang, X. Xie, Preparation of magnetic nanosphere/nanorod/nanosheet-like Fe_3O_4/Bi_2S_3/BiOBr with enhanced (001) and (110) facets to photodegrade diclofenac and ibuprofen under visible LED light irradiation, Chem. Eng. J., 378 (2019) 122169, doi: 10.1016/j.cej.2019.122169.
[23] T. Jia, J. Wu, J. Song, Q. Liu, J. Wang, Y. Qi, P. He, X. Qi, L. Yang, P. Zhao, *In-situ* self-growing 3D hierarchical BiOBr/$BiOIO_3$ Z-scheme heterojunction with rich oxygen vacancies and iodine ions as carriers transfer dual-channels for enhanced photocatalytic activity, Chem. Eng. J., 396 (2020) 125258, doi: 10.1016/j.cej.2020.125258.
[24] Z. Ye, X. Xiao, J. Chen, Y. Wang, Fabrication of $BiVO_4$/BiOBr composite with enhanced photocatalytic activity by a CTAB-assisted polyol method, J. Photochem. Photobiol., A, 368 (2019) 153–161.
[25] R. Dhanabal, S. Velmathi, A. Bose, Fabrication of RuO_2-Ag_3PO_4 heterostructure nanocomposites: investigations of band alignment on the enhanced visible light photocatalytic activity, J. Hazard. Mater., 344 (2018) 865–874.
[26] T. Li, H. Wei, H. Jia, T. Xia, X. Guo, T. Wang, L. Zhu, Mechanisms for highly efficient mineralization of bisphenol A by heterostructured Ag_2WO_4/Ag_3PO_4 under simulated solar light, ACS Sustainable Chem. Eng., 7 (2019) 4177–4185.
[27] X. Yu, J. Wang, X. Fu, H. Meng, Y. Zhu, Y. Zhang, Construction of Z-scheme $SrTiO_3$/Ag/Ag_3PO_4 photocatalyst with oxygen vacancies for highly efficient degradation activity towards tetracycline, Sep. Purif. Technol., 241 (2020) 116718, doi: 10.1016/j.seppur.2020.116718.
[28] Z. Shi, Y. Zhang, T. Liu, W. Cao, L. Zhang, M. Li, Z. Chen, Synthesis of BiOBr/Ag_3PO_4 heterojunctions on carbon-fiber cloth as filter-membrane-shaped photocatalyst for treating the flowing antibiotic wastewater, J. Colloid Interface Sci., 575 (2020) 183–193.
[29] B. Ju, F. Yang, K. Huang, Y. Wang, Fabrication, characterization and photocatalytic mechanism of a novel Z-scheme BiOBr/Ag_3PO_4@rGO composite for enhanced visible light photocatalytic degradation, J. Alloys Compd., 815 (2020) 151886, doi: 10.1016/j.jallcom.2019.151886.
[30] J. Li, X. Yang, C. Ma, Y. Lei, Z. Rui, Selectively recombining the photoinduced charges in bandgap-broken Ag_3PO_4/$GdCrO_3$ with a plasmonic Ag bridge for efficient photothermocatalytic VOCs degradation and CO_2 reduction, Appl. Catal., B, 291 (2021) 120053, doi: 10.1016/j.apcatb.2021.120053.
[31] R. Hou, Y. Gao, H. Zhu, G. Yang, W. Liu, Y. Huo, Z. Xie, H. Li, Coupling system of Ag/BiOBr photocatalysis and direct contact membrane distillation for complete purification of N-containing dye wastewater, Chem. Eng. J., 317 (2017) 386–393.
[32] G. Xu, M. Li, Y. Wang, N. Zheng, L. Yang, H. Yu, Y. Yu, A novel Ag-BiOBr-rGO photocatalyst for enhanced ketoprofen degradation: kinetics and mechanisms, Sci. Total Environ., 678 (2019) 173–180.
[33] X. Liu, L. Cai, Novel indirect Z-scheme photocatalyst of Ag nanoparticles and polymer polypyrrole co-modified BiOBr for photocatalytic decomposition of organic pollutants, Appl. Surf. Sci., 445 (2018) 242–254.
[34] Z. Shi, Y. Zhang, T. Liu, W. Cao, L. Zhang, M. Li, Z. Chen, Synthesis of BiOBr/Ag_3PO_4 heterojunctions on carbon-fiber cloth as filter-membrane-shaped photocatalyst for treating the flowing antibiotic wastewater, J. Colloid Interface Sci., 575 (2020) 183–193.
[35] Z. Chen, C. Huang, T. Zhou, J. Hu, Strike a balance between adsorption and catalysis capabilities in $Bi_2Se_{3-x}O_x$ composites for high-efficiency antibiotics remediation, Chem. Eng. J., 382 (2020) 122877, doi: 10.1016/j.cej.2019.122877.
[36] Z. Ye, X. Xiao, J. Chen, Y. Wang, Fabrication of $BiVO_4$/BiOBr composite with enhanced photocatalytic activity by a CTAB-assisted polyol method, J. Photochem. Photobiol., A, 368 (2019) 153–161.
[37] S. Huang, J. Zhong, J. Li, J. Chen, Z. Xiang, M. Li, Q. Liao, Charge separation and photocatalytic properties of BiOI prepared by ionic liquid-assisted hydrothermal method, Mater. Lett., 183 (2016) 248–250.
[38] B. Zhang, X. Hu, E. Liu, J. Fan, Novel S-scheme 2D/2D BiOBr/g-C_3N_4 heterojunctions with enhanced photocatalytic activity, Chin. J. Catal., 42 (2021) 1519–1529.
[39] H. Liu, J. Huang, J. Chen, J. Zhong, J. Li, R. Duan, Preparation and characterization of novel Ag/Ag_2WO_4/$ZnWO_4$ heterojunctions with significantly enhanced sunlight-driven photocatalytic performance, Solid State Sci., 95 (2019) 105923, doi: 10.1016/j.solidstatesciences.2019.06.012.
[40] T. Jia, J. Wu, Y. Xiao, Q. Liu, Q. Wu, Y. Qi, X. Qi, Self-grown oxygen vacancies-rich CeO_2/BiOBr Z-scheme heterojunction decorated with rGO as charge transfer channel for enhanced photocatalytic oxidation of elemental mercury, J. Colloid Interface Sci., 587 (2021) 402–416.
[41] H. Luo, M. Yan, Y. Wu, X. Lin, Y. Yan, Facile synthesis of PVDF photocatalytic membrane based on NCQDs/BiOBr/TiO_2 heterojunction for effective removal of tetracycline, Mater. Sci. Eng., B, 265 (2021) 114996, doi: 10.1016/j.mseb.2020.114996.
[42] D. Wu, T. Tsang, H. Yip, W. Wang, P. Wong, Highly efficient adhesion and inactivation of *Escherichia coli* on visible-light-driven amino-functionalized BiOBr hybrids, Environ. Res., 193 (2021) 110570, doi: 10.1016/j.envres.2020.110570.